



HAL
open science

Spin-orbit coupling induced ultrahigh-harmonic generation from magnetic dynamics

Ousmane Ly, Aurelien Manchon

► **To cite this version:**

Ousmane Ly, Aurelien Manchon. Spin-orbit coupling induced ultrahigh-harmonic generation from magnetic dynamics. *Physical Review B*, 2022, 105 (18), pp.L180415. 10.1103/PhysRevB.105.L180415 . hal-03830504

HAL Id: hal-03830504

<https://hal.science/hal-03830504>

Submitted on 26 Oct 2022

HAL is a multi-disciplinary open access archive for the deposit and dissemination of scientific research documents, whether they are published or not. The documents may come from teaching and research institutions in France or abroad, or from public or private research centers.

L'archive ouverte pluridisciplinaire **HAL**, est destinée au dépôt et à la diffusion de documents scientifiques de niveau recherche, publiés ou non, émanant des établissements d'enseignement et de recherche français ou étrangers, des laboratoires publics ou privés.

Spin-orbit coupling induced ultrahigh-harmonic generation from magnetic dynamics

Ousmane Ly^{1,*} and Aurelien Manchon^{1,2,†}

¹*Physical Science and Engineering Division (PSE), King Abdullah University of Science and Technology (KAUST), Thuwal 23955-6900, Saudi Arabia*

²*Aix-Marseille Univ, CNRS, CINaM, Marseille, France*

The generation of nonlinear high-frequency response in solids from powerful optical pumps has gained momentum over the past decade. High-harmonic generation in solids can be obtained from strong-field laser excitation, usually restricted to optical frequencies and limited both in amplitude and in harmonic order. Here, we demonstrate that high-harmonic emission can be achieved by exploiting conventional spin pumping, without the need for optical excitation. Considering a non-centrosymmetric (ferro- or antiferro-)magnet, we show that when the spin-orbit coupling strength is close to the s-d exchange energy, a strongly nonlinear regime resulting from resonant spin flip scattering occurs leading to the generation of a large number of harmonics at realistic precession frequencies, thereby enhancing both spin and charge dynamics by orders of magnitude. This mechanism could be used to trigger high-frequency emission deep in the THz regime.

Introduction - The recent boost in data transfer rates puts a daring strain on information technology. Sustaining such a growth rate requires the development of sources, detectors and systems working in the so-called TeraHertz (THz) gap covering the frequency window from 0.1 to 10 THz (1 THz = 10^{12} Hz). This gap represents a challenge for conventional electronic devices due to carrier transit delays (~ 1 -10ps), as well as for photonic devices due to thermal fluctuations (300K \sim 6THz). Nonetheless, designing efficient, room-temperature THz sources would constitute a key enabler to applications spanning from high-resolution imaging to extreme wide band wireless communication. The grand challenge posed by the THz gap is that it is located on the high-end of electronic processes and on the low-end of optical excitations. It is therefore difficult to emit THz electromagnetic field using purely electronic mechanisms because the scattering time of the electronic carriers is typically in the THz range. A successful strategy exploited in quantum cascade lasers is to use semiconductor superlattices with small gaps in order to generate the required frequency [1]. Since the efficiency is low, one needs to multiply the number of gaps (hence, the quantum cascade) and work at low temperature to quench thermal fluctuations. Another strategy is to exploit optical rectification of a femtosecond laser pulse in semiconductors like ZnTe [2]. An alternative approach uses an optically-generated ultrafast spin current, i.e., a charge-neutral current carrying spin angular momentum [3]. In this geometry, a femtosecond laser pulse impinges on the surface of a thin ferromagnetic film and excites a superdiffusive spin current [4]. This spin current then penetrates into an adjacent layer possessing large spin-orbit coupling and is subsequently converted into a charge current via either spin Hall effect [5] or Rashba-Edelstein effect [6], depending on the considered heterostructure. This apparatus enables the conversion of a femtosecond laser pulse into a THz electromagnetic field [3, 7, 8]. Although promising this solution relies on optical pumping and therefore

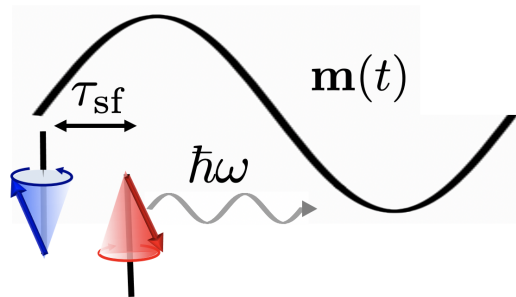


FIG. 1. (Color online) Spin-flip scattering driven high-harmonic generation: In the presence of a precessing magnetization order (gray line) the spin-orbit interaction leads to spin-flip scattering. Subsequently, a phase corresponding to the fundamental frequency is accumulated in the electronic wave-function. Under adiabatic magnetization dynamics, the spin flip time (τ_{sf}) becomes very small compared to the period of the precessing magnetic order, and higher harmonics appear as a consequence of subsequent spin flip scattering events during one fundamental cycle.

lacks scalability.

In this letter, we demonstrate that extremely efficient and ultrafast THz emission can be obtained by exploiting the internal dynamics of the spin-to-charge conversion to generate high-harmonics in a device solely powered by conventional magnetic resonance. The driving force is given by adiabatic spin pumping [9, 10], a widely used technique to generate pure spin currents out of ferromagnetic resonance, while the high-harmonic generation itself relies on the spin scattering events induced by spin-orbit coupling in the presence of a precessing magnetic order.

Spin pumping [9] is an adiabatic process by which a precessing magnetic order $\mathbf{m}(t)$ (ferromagnetic or antiferromagnetic alike) injects a spin current into an adjacent metallic layer. This spin current possesses two components, a rectified one whose spin polarization is aligned along the precession axis $\mathcal{J}_s \sim \langle \mathbf{m} \rangle$, and an os-

cillating contribution whose spin polarization is aligned perpendicular to the precession axis $\mathcal{J}_s \sim \mathbf{m} \times \partial_t \mathbf{m}$. In a conventional spin pumping experiment, once injected in the normal metal, this spin current is converted into a charge current via spin-orbit coupling [10–12], which leads to the dc and ac components depicted on Fig. 2(a). This spin-to-charge conversion does not affect the spin dynamics itself as long as the spin-orbit coupling is negligible compared to the s-d exchange, and thereby only generates a harmonic charge current.

In the presence of spin-orbit coupling though, successive spin flip events occur within one magnetic precession cycle, leading to the appearance of higher frequencies in the charge current signal (see Fig. 1). Subsequently, a phase corresponding to the dynamic frequency is accumulated as a consequence of angular momentum conservation. When the spin-orbit coupling energy becomes comparable to the s-d exchange parameter, the full harmonic spectrum is excited with extremely strong amplitudes. This is in close analogy with the high-harmonic generation mechanism from gaseous media under Laser excitation [13–15], where the electron wave-packets undergo harmonic emission as they re-collide to their parent atoms after a fraction of the Laser oscillation cycle. When the magnetization dynamics operates at small frequencies the emission of a huge number of harmonics is predicted.

Interestingly, our numerical simulations suggest the existence of a resonance condition associated to maximally excited high-harmonics. This corresponds to the regime where the s-d exchange energy is very close to the spin-orbit splitting. While the effect is not restricted to a particular type of spin-orbit interaction, the Rashba-like spin-orbit coupling constitutes a central paradigm to demonstrate the proposed effect. In fact, Rashba spin-orbit interaction has been found in a broad range of magnetic interfaces, from transition metal interfaces [10], to the surface of topological insulators [16] or in oxide heterostructures [17], and has the major advantage of being electrically tunable [18], offering a powerful means to control the high-harmonic generation.

Numerical simulations - To demonstrate the high-harmonic generation, we consider the setup depicted on Fig. 2(b). The numerical calculations are performed using the time dependent quantum transport package T-KWANT [19–21] where the stationary scattering properties are obtained from the dc transport package KWANT [22]. We consider a two dimensional tight binding model including both exchange and Rashba spin-orbit coupling. The underlying Hamiltonian is given by

$$\mathcal{H}(t) = \mathcal{H}_0(t) + \mathcal{H}_R, \quad (1)$$

where,

$$\mathcal{H}_0(t) = J \sum_r \hat{c}_r^\dagger (\hat{\sigma} \cdot \mathbf{m}(r, t)) \hat{c}_r - \gamma \sum_{\langle r, r' \rangle} (\hat{c}_r^\dagger \hat{c}_{r'} + \text{h.c.}), \quad (2)$$

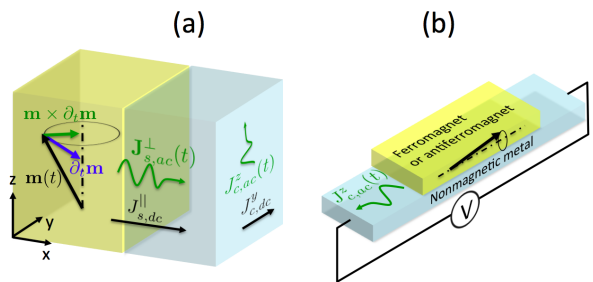


FIG. 2. (Color online) Illustration of the spin pumping setup: (a) Schematics of the d.c. and a.c. spin pumping: a magnetic order precessing around its rest direction \mathbf{z} induces a spin current composed of a d.c. component, $\mathcal{J}_{s,dc}^\parallel$ (black), and an a.c. (green) component, $\mathcal{J}_{s,ac}^\perp$, whose spin polarization is aligned on $\mathbf{m} \times \partial_t \mathbf{m}$. We neglect the contribution from the imaginary part of the spin mixing conductance ($\sim \partial_t \mathbf{m}$). Via spin-orbit coupling, these spin currents are converted into a d.c. and an a.c. charge current flowing along \mathbf{y} and \mathbf{z} , respectively. (b) Corresponding simulation setup: the pumped charge current is collected along the direction about which the magnetic order precesses.

with h.c standing for hermitian conjugate, $\mathbf{m}(r, t)$ being the time dependent magnetization which also depends on position in the case of the antiferromagnetic dynamics. J is the s-d exchange energy between the conduction electrons and the local magnetic order. The operator $\hat{\sigma}$ represents the vector of Pauli matrices and γ the tight binding hopping energy. The operators \hat{c}_r^\dagger and \hat{c}_r are respectively the creation and annihilation operators at position r given by the coordinates x and y . The Rashba Hamiltonian is given by

$$\mathcal{H}_R = i\gamma \left(\frac{\alpha_R}{2} \right) \sum_r \hat{c}_{x,y}^\dagger (\hat{\sigma}_y \hat{c}_{x+1,y} - \hat{\sigma}_x \hat{c}_{x,y+1}) + \text{h.c.}, \quad (3)$$

with α_R the Rashba parameter. The system is connected to two transversal normal leads that allows for probing the pumped currents, see Fig. 2(b).

To compute the non-equilibrium charge current, the stationary scattering modes of the tight binding system at different energies are obtained using KWANT. Subsequently, they are evolved forward in time according to the time dependent Schrödinger equation,

$$i\hbar \partial_t \Psi_{\eta m \varepsilon}(t) = \mathcal{H}(t) \Psi_{\eta m \varepsilon}(t), \quad (4)$$

where η stands for the lead from which the state originates, m is the mode index and ε is the transport energy. Furthermore, the time dependent current at temperature T is obtained as

$$I(t) = \sum_{\eta m} \int \frac{d\varepsilon}{2\pi} f(\varepsilon, T) \Psi_{\eta m \varepsilon}^\dagger(t) \Psi_{\eta m \varepsilon}(t), \quad (5)$$

with $f(\varepsilon, T)$ being the Fermi distribution function at energy ε and temperature T .

All the numerical calculations are performed at a chemical potential of 100 meV. Therefore, the calculated currents are summed from the bottom of the bands to the considered energy. The s-d exchange coupling and the temperature of the system are set to $J = 500$ meV and $T = 0$ K respectively, except otherwise stated. To obtain the charge currents in the frequency domain, a discrete fast Fourier transform of the time dependent signal is performed. In the data presented throughout the text I_ω represents the absolute value of the normalized Fourier transform of $I(t)$ given by Eq. (5). Further, we emphasize that the present effect is independent on the nature of the magnetic resonance and is only governed by the ratio of the spin-orbit coupling strength to the dynamic frequency. In fact, the high-harmonic generation is obtained for both ferromagnetic and antiferromagnetic resonances (see Supplemental information [23]). Nonetheless, in the numerical method we use, the simulation time is set by the electron's energy and is of the order of the hopping parameter γ (typically of the order of 0.1 eV). In order to keep the computational cost reasonable, we have to consider a magnetic system whose resonance frequency is only two orders of magnitude smaller than the internal dynamics of the conduction spin. To comply with the numerical constraints, we therefore consider antiferromagnetic resonance (typically \sim meV) rather than ferromagnetic resonance (typically \sim μ eV). We stress out that this does not affect the generality of our results.

In antiferromagnetic resonance the two sublattice magnetization vectors, \mathbf{m}_1 and \mathbf{m}_2 , undergo different precession modes of opposite chirality [24]. Without loss of generality, we consider the right-handed polarization of the order parameter, in which case both sublattice vectors rotate anticlockwise [25]. As a result, the antiferromagnet order parameter $\mathbf{n} = (\mathbf{m}_1 - \mathbf{m}_2)/2$ precesses with the same chirality and a non-zero, albeit small, in-plane magnetization $\mathbf{m} = (\mathbf{m}_1 + \mathbf{m}_2)/2$ develops. As the sublattice magnetizations precess in time, the spin current pumped out of the antiferromagnet reads [24],

$$\mathcal{J}_s = \Re\{g^{\uparrow\downarrow}\} (\mathbf{m} \times \partial_t \mathbf{m} + \mathbf{n} \times \partial_t \mathbf{n}) - \Im\{g^{\uparrow\downarrow}\} \partial_t \mathbf{m}, \quad (6)$$

where $g^{\uparrow\downarrow}$ is the interfacial spin mixing conductance. The symbols $\Re\{\dots\}$ and $\Im\{\dots\}$ stand for real and imaginary parts, respectively. In contrast to the ferromagnetic case, the spin current pumped out of an antiferromagnetic metal decomposes into a couple of a.c. spin currents: a ferromagnetic like contribution \mathcal{J}_m^s along the precession cone axis, given by the first and last terms of Eq. (6), and a staggered contribution \mathcal{J}_n^s rotating in the (x, y) plane, given by the second term of Eq. (6). In the region subjected to the spin-orbit interaction, the two a.c. spin current contributions are converted into a.c. charge currents in both y and z directions according to the inverse spin Hall effect [11].

High-harmonic generation from adiabatic pumping - The time dependence of the collected current is displayed

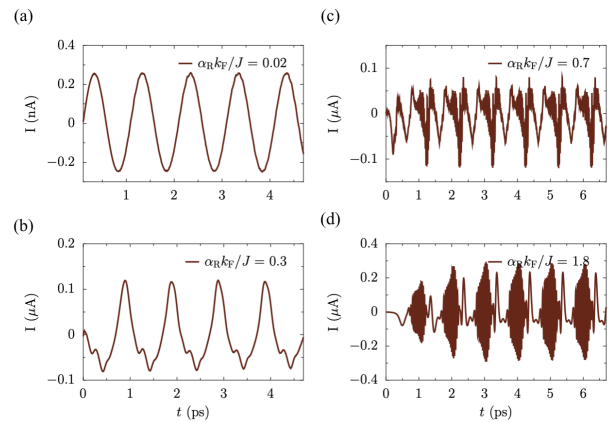


FIG. 3. (Color online) Time domain current signal as a function of Rashba strength: Time dependent currents for different spin-orbit coupling strengths are displayed. Here, an exchange coupling of $J = 500$ meV is taken and the precession angle is set at $\theta = 10^\circ$. Considering a lattice spacing of 5 Å the value of α_R at $\alpha_R k_F / J = 1$ corresponds to 3.57 eV Å, which is very close to its value in Bi/Ag alloys [26] or in other bismuth based topological insulators [27].

on Fig. 3 for different Rashba strengths. We immediately identify three main regimes. For $\alpha_R k_F / J \ll 1$, the current response is dominated by oscillations of frequency ω [Fig. 3(a)]. When the Rashba parameter becomes comparable to the s-d exchange, $\alpha_R k_F / J \sim 1$, the magnitude of the a.c. current substantially increases whereas involving oscillations with higher frequencies. Upon further increasing the Rashba parameter, $\alpha_R k_F / J > 1$, the amplitude of the signal decreases substantially with very weak components of the higher harmonics. Further numerical simulations suggest the reappearance of the highly excited harmonics regime when $\alpha_R k_F / J \gg 1$. However, the underlying parameter space corresponds to unrealistic spin-orbit coupling strengths.

For a more quantitative discussion, we report in Fig. 4 the Fourier transform of the charge current signals for different values of α_R . For $\alpha_R k_F / J \ll 1$ [Fig. 4(a)], the signal exhibits only one frequency, although we do observe the appearance of the two lowest harmonics. This is consistent with the adiabatic spin pumping theory [9, 10]. Upon increasing the Rashba strength [Fig. 4(b) and 4(c)], higher harmonics progressively emerge with amplitudes slightly below the fundamental frequencies. Notice that the amplitudes of the higher harmonics are only one order of magnitude smaller than the fundamental harmonic at frequency ω . For the sake of comparison, Ref. 28 recently reported the optical generation of higher harmonics in graphene driven by internal electron thermalization. The authors observed harmonics up to the seventh order with amplitudes four orders of magnitude smaller than that of the fundamental mode. In contrast, our simulations demonstrate that the first few harmonics remain of the order as the fundamental frequency in this

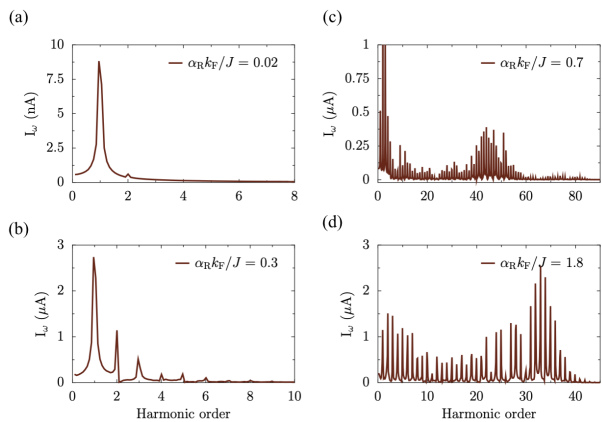


FIG. 4. (Color online) Frequency domain charge current as a function of Rashba strength: Fourier amplitudes of the charge current are shown at different spin-orbit strengths in both perturbative and non perturbative regimes. The anti-ferromagnetic dynamics parameters are the same as in Fig. 3.

regime. Upon reaching the resonance, even higher number of harmonics are generated. We emphasize that at resonance, our simulations yield signals with amplitudes increasing in time. This peculiar behavior may result from convergence issues related to the resonance condition. Nonetheless, similar features have been recently reported in correlated electron systems [29]. Therefore, we believe that this particular parameter space deserves further investigations. Above resonance though, when $\alpha_R k_F / J > 1$ [Fig. 4(d)], the current response still display a large number of harmonics.

In order to offer a comprehensive picture of the high-harmonic generation, the current output is reported on Fig. 5 as a function of the spin-orbit strength $\alpha_R k_F / J$ and the harmonic order, the amplitude of the harmonic being given by the color scale. The resonance regime corresponding to the ultrahigh-harmonic generation is centered around $\alpha_R k_F / J = 1$ and extends from $\alpha_R k_F / J \approx 0.8$ to $\alpha_R k_F / J \approx 1.2$, indicating that the effect is robust against material's parameters variations and thereby providing a wide region of tunability. As a matter of fact, we observed that the signal bandwidth is proportional to the driving frequency ($\propto 1/\omega$), as shown in Fig. 6(a). Further, it is worth emphasizing that the precession cone opening plays a crucial role in enhancing the amplitudes of the highest harmonics. Although Fig. 6(a) predicts an emission up to the 500th harmonic for the dynamic frequency considered in Fig. 5, only about a hundred of them exhibit strong enough amplitudes for the precession angle considered (here, $\theta = 10^\circ$). At larger precession angles all the higher harmonics can be excited with amplitudes comparable to the first harmonic intensity (see [23]).

On the contrary, upon reducing the pumping fre-

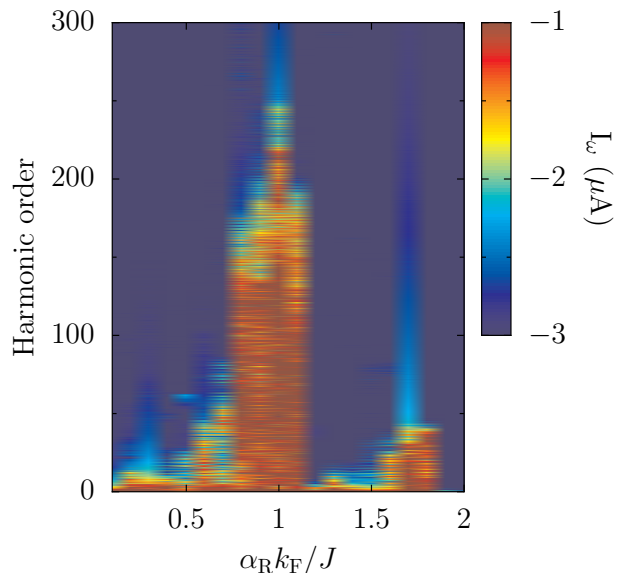


FIG. 5. (Color online) Charge current amplitude of the harmonic spectrum as a function of spin-orbit strength: The current amplitude (in logarithmic scale) is shown as a function of the Harmonic order as well as the Rashba strength. The frequency of the dynamics as well as the precession angle are the same as in Fig. 3.

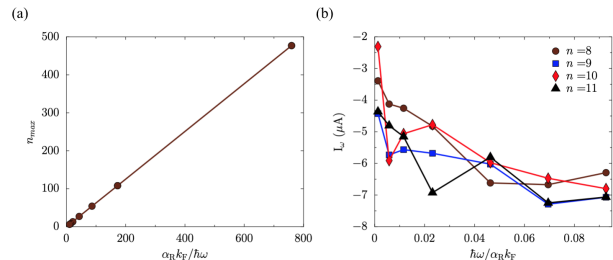


FIG. 6. (Color online) Emission bandwidth and charge current amplitude as a function of the driving frequency: (a) Maximum number of harmonics as a function of the inverse of the fundamental frequency. (b) Amplitude of selected harmonics as a function of the driving frequency. The Rashba strength is tuned to the maximally excited regime.

quency, one can substantially enhance the number of harmonics. This is illustrated in [23], where the Fourier spectrum of the charge current computed for a driving frequency of 0.4 THz is shown. We notice that a similar decay of the number of the generated harmonics with respect to ω has been reported in different solid state systems under intense laser excitation [30–32].

Discussion - A crucial question we now wish to comment on is the applicability of our single-orbital model to realistic systems. As mentioned in the introduction, adiabatic spin-to-charge conversion has been demonstrated in a wide variety of heterostructures accommodating both Rashba-like spin-orbit coupling and s-d exchange. Transition metal ferromagnets interfaced with topological

insulators[16] and oxide heterostructures[18] are among the most promising structures. In these systems, Rashba-like spin-orbit coupling arises from a complex interfacial orbital hybridization scheme that is essentially overlooked in our model. Nonetheless, intense theoretical investigation on spin-orbit physics[33] (spin-orbit torque and spin-to-charge conversion) has established that in spite of its simplicity, modeling the interfacial spin-orbit coupling by an effective Rashba interaction is sufficient to properly describe the physics at stake and obtain reasonable orders of magnitude. Furthermore, the robustness of the effect at room temperature is of great relevance in terms of the applicability of the effect to real devices.

The present effect opens appealing perspectives for high frequency emission deep into the THz gap. It is worth emphasizing that the effect requires two essential ingredients: strong spin-orbit coupling and oscillating magnetic order or magnetic field with in-plane components. Note that recent simulations based on the present work have reproduced high harmonic generation on 1-dimensional magnetic chain, although using a different configuration setup [34] at low s-d exchange coupling.

Now we discuss the possible experimental realization of our proposal. We stress out that conventional spin-to-charge conversion heterostructures are suitable platforms to harness the effect. In fact, the very nature of Rashba spin-orbit coupling makes this perspective quite appealing because it is directly related to the interfacial potential drop and therefore highly sensitive to a gate voltage for instance. Whereas this electrical tuning of the Rashba strength has been demonstrated in several systems, oxide two-dimensional electron gases [18, 35, 36] stand out of the most versatile system. The recent demonstration of electrical switching of Rashba coupling [36] makes this perspective even more compelling. The Rashba strength can be as large as a few 100 meV, which seems reasonable as the effective s-d exchange experienced on the surface can be tuned by inserting a tunnel barrier for instance. Furthermore, a strong enhancement of spin-orbit coupling strength in graphene to 80 meV has been recently reported [37], where the spin-orbit coupling strength can be controlled in a field effect transistor setup. This provides a variety of systems in which the effect can be observed.

The authors acknowledge useful discussions with X. Waintal and B. Nikolic, as well as computing resources on the supercomputer SHAHEEN granted by the KAUST Supercomputing Lab. O. L thanks A. Abbout for useful discussions. This work was supported by the King Abdullah University of Science and Technology (KAUST) through the Office of Sponsored Research (OSR) [Grant Number OSR-2020-CRG8-4048].

* ousmane.ly@kaust.edu.sa

† aurelien.manchon@univ-amu.fr

- [1] Benjamin S Williams, “Terahertz quantum-cascade lasers,” *Nature Photonics* **1**, 517 (2007).
- [2] M. Tonouchi, “Cutting-edge terahertz technology,” *Nature Photonics* **1**, 97 (2007).
- [3] T. Seifert, S. Jaiswal, U. Martens, J. Hannegan, L. Braun, P. Maldonado, F. Freimuth, A. Kronenberg, J. Henrzi, I. Radu, E. Beaupaire, Y. Mokrousov, P. M. Oppeneer, M. Jourdan, G. Jakob, D. Turchinovich, L. M. Hayden, M. Wolf, M. Münzenberg, M. Kläui, and T. Kampfrath, “Efficient metallic spintronic emitters of ultrabroadband terahertz radiation,” *Nature Photonics* **10**, 483 (2016), [arXiv:1510.03729](https://arxiv.org/abs/1510.03729).
- [4] M Battiato, K Carva, and P M Oppeneer, “Superdiffusive Spin Transport as a Mechanism of Ultrafast Demagnetization,” *Physical Review Letters* **105**, 027203 (2010).
- [5] Jairo Sinova, Sergio O. Valenzuela, J. Wunderlich, C. H. Back, and T. Jungwirth, “Spin Hall effect,” *Review of Modern Physics* **87**, 1213 (2015).
- [6] V M Edelstein, “Spin Polarization of conduction electrons induced by electric current in two-dimensional asymmetric electron systems,” *Solid State Communications* **73**, 233 (1990).
- [7] Tobias Kampfrath, M Battiato, P Maldonado, G Eilers, J Nötzold, S Mährlein, V Zbarsky, Frank Freimuth, Yuriy Mokrousov, Stefan Blügel, M Wolf, I Radu, P M Oppeneer, and M. Münzenberg, “Terahertz spin current pulses controlled by magnetic heterostructures.” *Nature Nanotechnology* **8**, 256 (2013).
- [8] T J Huisman, R V Mikhaylovskiy, J D Costa, F Freimuth, E Paz, J Ventura, P P Freitas, S Blügel, Y Mokrousov, Th. Rasing, and A V Kimel, “Femtosecond control of electric currents in metallic ferromagnetic heterostructures,” *Nature Nanotechnology* **11**, 455 (2016), [arXiv:1505.02970](https://arxiv.org/abs/1505.02970).
- [9] Arne Brataas, Yaroslav Tserkovnyak, G. E. W. Bauer, and Bertrand Halperin, “Spin battery operated by ferromagnetic resonance,” *Physical Review B* **66**, 060404 (2002).
- [10] E. Saitoh, M. Ueda, H. Miyajima, and G. Tatara, “Conversion of spin current into charge current at room temperature: Inverse spin-Hall effect,” *Applied Physics Letters* **88**, 182509 (2006).
- [11] Dahai Wei, Martin Obstbaum, Mirko Ribow, C. H. Back, and Georg Woltersdorf, “Spin Hall voltages from a.c. and d.c. spin currents.” *Nature Communications* **5**, 3768 (2014).
- [12] J C Rojas-Sánchez, L Vila, G Desfonds, S Gambarelli, J.-P. Attane, J M De Teresa, C Magén, and A. Fert, “Spin-to-charge conversion using Rashba coupling at the interface between non-magnetic materials.” *Nature Communications* **4**, 2944 (2013).
- [13] P. B. Corkum, “Plasma perspective on strong field multiphoton ionization,” *Phys. Rev. Lett.* **71**, 1994–1997 (1993).
- [14] P. B. Corkum and Ferenc Krausz, “Attosecond science,” *Nature Physics* **3**, 381–387 (2007).
- [15] Katsumi Midorikawa, “Ultrafast dynamic imaging,” *Nature Photonics* **5**, 640–641 (2011).
- [16] Y. Shiomi, K. Nomura, Y. Kajiwara, K. Eto, M. No-

- vak, Kouji Segawa, Yoichi Ando, and E. Saitoh, “Spin-Electricity Conversion Induced by Spin Injection into Topological Insulators,” *Physical Review Letters* **113**, 196601 (2014).
- [17] A. D. Caviglia, M. Gabay, S. Gariglio, N. Reyren, C. Cancellieri, and J.-M. Triscone, “Tunable Rashba Spin-Orbit Interaction at Oxide Interfaces,” *Phys. Rev. Lett.* **104**, 126803 (2010).
- [18] Diogo C Vaz, Paul Noël, Annika Johansson, Börge Göbel, Flavio Y Bruno, Gyanendra Singh, Siobhan Mckeown-walker, Felix Trier, Luis M Vicente-arche, Anke Sander, Sergio Valencia, Pierre Bruneel, Manali Vivek, Marc Gabay, Nicolas Bergeal, Felix Baumberger, Hanako Okuno, Agnès Barthélémy, Albert Fert, Laurent Vila, Ingrid Mertig, Jean-philippe Attané, and Manuel Bibes, “Mapping spin-charge conversion to the band structure in a topological oxide two-dimensional electron gas,” *Nature Materials* **18**, 1187 (2019).
- [19] Joseph Weston and Xavier Waintal, “Linear-scaling source-sink algorithm for simulating time-resolved quantum transport and superconductivity,” *Physical Review B* **93**, 134506 (2016).
- [20] Benoit Gaury, Joseph Weston, Matthieu Santin, Manuel Houzet, Christoph Groth, and Xavier Waintal, “Numerical simulations of time-resolved quantum electronics,” (2014).
- [21] Thomas Kloss, Joseph Weston, Benoit Gaury, Benoit Rossignol, Christoph Groth, and Xavier Waintal, “Tk-want: a software package for time-dependent quantum transport,” *New Journal of Physics* **23**, 023025 (2021).
- [22] Christoph W. Groth, Michael Wimmer, Anton R. Akhmerov, and Xavier Waintal, “Kwant: A software package for quantum transport,” *New Journal of Physics* **16**, 063065 (2014), arXiv:1309.2926.
- [23] “Supplemental Materials.”
- [24] Ran Cheng, Jiang Xiao, Qian Niu, and Arne Brataas, “Spin pumping and spin-transfer torques in antiferromagnets,” *Physical Review Letters* **113**, 057601 (2014).
- [25] F. Keffer and C. Kittel, “Theory of Antiferromagnetic Resonance,” *Phy. Rev.* **85**, 329 (1952).
- [26] Christian Ast, Jürgen Henk, Arthur Ernst, Luca Moreschini, Mihaela Falub, Daniela Pacilé, Patrick Bruno, Klaus Kern, and Marco Grioni, “Giant Spin Splitting through Surface Alloying,” *Phys. Rev. Lett.* **98**, 186807 (2007).
- [27] Haijun Zhang, Chao-Xing Liu, Xiao-Liang Qi, Xi Dai, Zhong Fang, and Shou-Cheng Zhang, “Topological insulators in Bi_2Se_3 , Bi_2Te_3 and Sb_2Te_3 with a single Dirac cone on the surface,” *Nature Physics* **5**, 438–442 (2009).
- [28] Hassan A Hafez, Sergey Kovalev, Jan-christoph Deinert, Zoltán Mics, Bertram Green, Nilesh Awari, Min Chen, Semyon Germanskiy, Ulf Lehnert, Jochen Teichert, Zhe Wang, Klaas-jan Tielrooij, Zhaoyang Liu, Zongping Chen, Akimitsu Narita, Klaus Müllen, Mischa Bonn, Michael Gensch, and Dmitry Turchinovich, “Extremely efficient terahertz high-harmonic generation in graphene by hot Dirac fermions,” *Nature* **56**, 507 (2018).
- [29] Shohei Imai, Atsushi Ono, and Sumio Ishihara, “High Harmonic Generation in a Correlated Electron System,” *Physical Review Letters* **124**, 157404 (2020).
- [30] Shambhu Ghimire and David A. Reis, “High-harmonic generation from solids,” *Nature Physics* **15**, 10–16 (2019).
- [31] T. T. Luu, M. Garg, S. Yu Kruchinin, A. Moulet, M. Th Hassan, and E. Goulielmakis, “Extreme ultraviolet high-harmonic spectroscopy of solids,” *Nature* **521**, 498–502 (2015).
- [32] Mengxi Wu, Shambhu Ghimire, David A. Reis, Kenneth J. Schafer, and Mette B. Gaarde, “High-harmonic generation from Bloch electrons in solids,” *Phys. Rev. A* **91**, 043839 (2015).
- [33] A Manchon, J. Zelezny, M. Miron, Tomáš Jungwirth, Jairo Sinova, André Thiaville, Kevin Garello, and Pietro Gambardella, “Current-induced spin-orbit torques in ferromagnetic and antiferromagnetic systems,” *Review of Modern Physics* **91**, 035004 (2019).
- [34] J. Varela Manjarres, O. Ly, A. Manchon, T. Kloss, X. Waintal, and B. K. Nikolic, “High-harmonic generation in spin and charge current pumping at ferromagnetic or antiferromagnetic resonance in the presence of spin-orbit coupling,” (2021), arXiv:arXiv:2112.14685.
- [35] E. Lesne, Yu Fu, S. Oyarzun, J. C. Rojas-Sánchez, D. C. Vaz, H. Naganuma, G. Sicoli, J. P. Attané, M. Jamet, E. Jacquet, J. M. George, A. Barthélémy, H. Jaffrès, A. Fert, M. Bibes, and L. Vila, “Highly efficient and tunable spin-to-charge conversion through Rashba coupling at oxide interfaces,” *Nature Materials* **15**, 1261 (2016).
- [36] Paul Noël, Felix Trier, Luis M Vicente Arche, Julien Bréhin, Diogo C Vaz, Vincent Garcia, Stéphane Fusil, Agnès Barthélémy, Laurent Vila, Manuel Bibes, and Jean-philippe Attané, “Non-volatile electric control of spin-to-charge conversion in a SrTiO_3 Rashba system,” *Nature* **580**, 483 (2020).
- [37] Amir Muhammad Afzal, Kuen Hong Min, Byung Min Ko, and Jonghwa Eom, “Observation of giant spin-to-charge conversion in graphene and heavy metal heterostructures,” *RSC Adv.* **9**, 31797–31805 (2019).